ELSEVIER

Nuclear Engineering and Design 223 (2003) 75–102

Nuclear Engineering and Design

www.elsevier.com/locate/nucengdes

Ex-vessel corium spreading: results from the VULCANO spreading tests

Christophe Journeau*, Eric Boccaccio, Claude Brayer, Gérard Cognet[1], Jean-François Haquet, Claude Jégou, Pascal Piluso, José Monerris

Commissariat à l'Energie Atomique, CEA/Cadarache, Severe Accident Mastering Laboratory (DEN/DTP/STH/LMA) F13108 St. Paul lez Durance, France

Received 9 April 2002; received in revised form 23 October 2002; accepted 6 December 2002

Abstract

In the hypothetical case of a nuclear reactor severe accident, the reactor core could melt and form a mixture, called corium, of highly refractory oxides (UO_2, ZrO_2) and metallic or oxidized steel, that could eventually flow out of the vessel and mix with the basemat decomposition products (generally oxides such as SiO_2, Al_2O_3, CaO, Fe_2O_3, . . .). For some years, the French Atomic Energy Commission (CEA) has launched an R&D program which aimed at providing the tools for improving the mastering of severe accidents.

Within this program, the VULCANO experimental facility is operated to perform experiments with prototypic corium (corium of realistic chemical composition including depleted UO_2). This is coupled with the use of specific high-temperature instrumentation requiring in situ cross calibration. This paper is devoted to the "spreading experiments" performed in the VULCANO facility, in which the effects of flow and solidification are studied.

Due to the complex behavior of corium in the solidification range, an interdisciplinary approach has been used combining thermodynamics of multicomponent mixtures, rheological models of silicic semisolid materials, heat transfer at high temperatures, free-surface flow of a fluid with temperature-dependant properties.

Twelve high-temperature spreading tests have been performed and analyzed. The main experimental results are the good spreadability of corium–concrete mixtures having large solidification ranges even with viscous silicic melts, the change of microstructure due to cooling rates, the occurrence of a large thermal contact resistance at the corium–substrate interface, the presence of a steep viscosity gradient at the surface, the transient concrete ablation. Furthermore, the experiments showed the presence of the gaseous inclusions in the melt even without concrete substrate. This gas release is linked to the local oxygen content in the melt which is function of the nature of the atmosphere, of the phases (FeO_x, UO_y, . . .) and of the substrate. These tests with prototypic material have improved our knowledge on corium and contributed to validate spreading models and codes which are used for the assessment of corium mastering concepts.

1. Introduction

Nuclear fission energy provides about 80% of the electricity supply in France and 33% in the European Union. It has several important strategic benefits: independence from fossil fuels, long-term security of primary energy supply and zero emission of

* Corresponding author.

E-mail addresses: christophe.journeau@cea.fr (C. Journeau), eric.boccaccio@cea.fr (E. Boccaccio), gerard.cognet@cea.fr (G. Cognet), haquet@eloise.cad.cea.fr (J.-F. Haquet), claude.jegou@cea.fr (C. Jégou), pascal.piluso@cea.fr (P. Piluso), jose.monerris@cea.fr (J. Monerris).

[1] Present address: CEA/Saclay, DEN/DSNI, F91191 Gif sur Yvette, France.

0029-5493/02/$ – see front matter © 2002 Elsevier Science B.V. All rights reserved.
doi:10.1016/S0029-5493(02)00397-7

greenhouse-effect gases. These advantages make, certainly, nuclear energy the best choice for electricity production in the future. However, according to the consequences of a severe accident, even if it has a very low probability, it is always needed to increase the safety levels. Consequently, this implies the improvement of knowledge with the view to simultaneously increasing safety and maintaining competitiveness.

Since the Three Miles Island accident in 1979 (e.g. Broughton et al., 1989) and especially since the Chernobyl accident in 1986 (e.g. Pazukhin, 1994), it is clear that one of the key points to increase safety is that any reasonably credible accident must be controlled within the reactor containment with no off-site consequences. In this context, for some years now, the CEA has undertaken a large program on severe accidents (Cognet et al., 1997) which aims at providing the tools for their mastering in both existing and future power plants.

For the European pressurized water reactor (EPR) project, core melt accident is one of the severe accidents to be mastered under the new safety approach for the reactor design. Therefore, a dedicated area of about 175 m^2 (Weisshäupl, 1999) has been devoted to the spreading of the molten mixture called *corium*, essentially composed of uranium, zirconium and silicon dioxides and of more or less oxidized steel, that would result from the hypothetical melting down of the core, melting through the reactor vessel and mixing with a sacrificial concrete in the reactor pit. The role of spreading is to reduce the surface thermal load due to the radioactive decay heat.

To study corium spreading, a series of experiments have been performed. The first reported experiments, at Brookhaven National Laboratory (Greene et al., 1988) were conducted with lead as simulant. The CORINE facility (Vetau et al., 1996) has been built for low temperature analytic experiments with aqueous or metallic simulants. Low temperature simulant spreading experiments have also been performed for volcanological applications (Fink and Griffiths, 1990). The Scaled Simulant Spreading Experiments (S3E) enabled spreading experiments to be performed at temperatures up to 1100 °C (Dinh et al., 2000). In the SPREAD (Suzuki et al., 1993) and KATS facilities (Fieg et al., 1996) alumina above 1700 °C was used as a simulant.

Spreading experiments using prototypic corium, i.e. melt containing depleted uranium dioxide with the composition of a hypothetic severe accident scenario, have been performed in the CARLA (Sappok and Steinwarz, 1999), FARO (Tromm et al., 2000) and VULCANO (Cognet et al., 1999) facilities. Due to the specific properties of uranium dioxide (material properties, oxidation states, existence of volatile uranium oxides at normal pressure and relatively low temperatures, . . .) the use of prototypic corium compositions is absolutely necessary to validate works done with simulants (Piluso et al., 2001).

This paper presents the VULCANO facility and the main results from the spreading tests that have been conducted there. They have been obtained through an interdisciplinary approach linking heat transfer, fluid mechanics, physico-chemistry, materials science and thermodynamics. Rather than focusing on specific experiments or techniques, this paper synthesizes the various data and results obtained in this test series.

2. The VULCANO facility

The VULCANO facility (Cognet et al., 1999) is mainly composed of a furnace (Jégou et al., 1998) and a test section, which is thoroughly instrumented. Post-test analyses, which are a necessary part of prototypic corium tests, will also be described. An interdisciplinary experimental team operates this facility within the PLINIUS experimental platform at CEA Cadarache. This prototypic corium platform is currently unique in the European Union.

2.1. The furnace

To achieve experiments with prototypic material, the furnace has the following characteristics:

- Capability to melt oxidic mixtures of various compositions (UO_2, ZrO_2, SiO_2, FeO_x) with the possible addition of metals.
- Liquidus temperature of the load between 1700 and 2900 °C.
- Capacity to melt and to pour 100 kg.
- Continuous low pouring rates (0.1–1 l/s).

A study of the candidate technologies with respect of these requirements lead to the choice of a transferred plasma-arc furnace. Two plasma torches are ignited by an electrical short circuit. The main arc

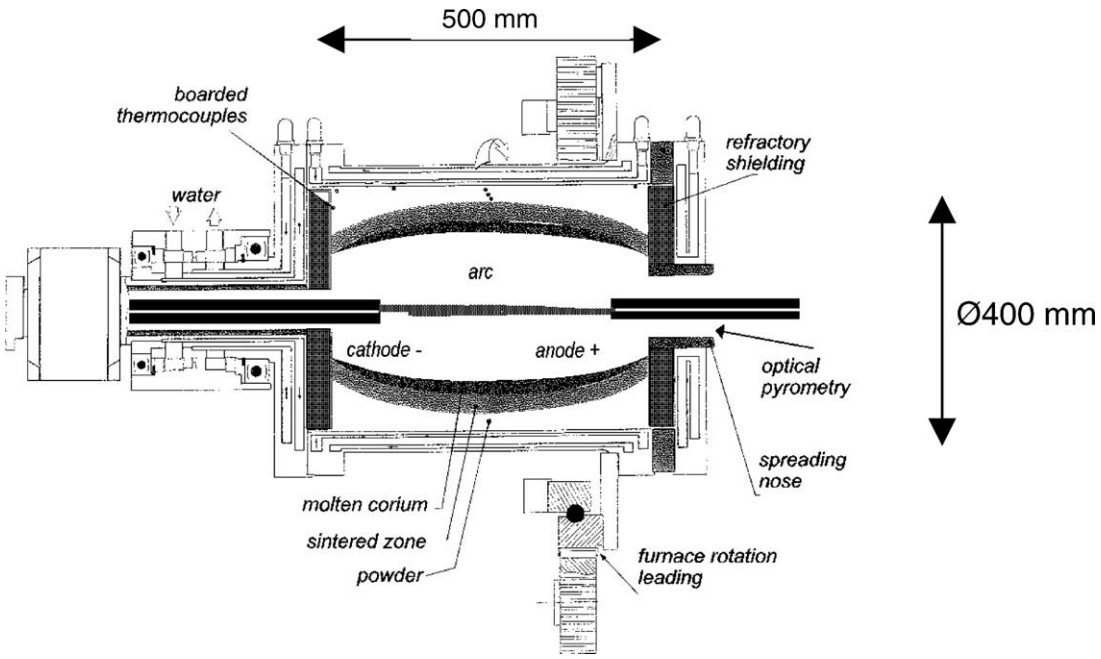

Fig. 1. The VULCANO furnace.

is then created and transferred between these two torches having opposite polarity (see Fig. 1). The electrode tips are made of graphite. The plasmagenic gas is composed of argon and/or nitrogen plus, in some cases, corium fumes. The maximum available power is around 600 kW (1000 A and 600 V). For our practical operating condition, the maximum arc voltage is of 300 V, i.e. an effective maximum power of 300 kW.

The mixtures to melt are introduced under the form of powders in a cylindrical rotating cavity (400 mm diameter and 500 mm long). In order to protect the furnace steel walls, a self-crucible of zirconia is realized in the furnace by the centrifugation (between 150 and 300 rpm) and heating of partially stabilized zirconia powder. The furnace external surfaces are water-cooled while the inner surface of the load is subject to the radiation from the plasma arc (temperatures between 10,000 and 20,000 °C). Radiation heats the surface, then, convection and mainly conduction transfer the heat to the inner layers. In the zirconia self crucible, there are then three distinctive layers (from center to periphery): molten material, sintered zone and cold powder. The corium powder is then loaded and molten. Two successive phases of loading and melting are used in order to increase the furnace effective capacity by compensating for the powder low density compared to that of a molten material.

The heating process is controlled by optical pyrometry and in-board embedded thermocouples. When a sufficient quantity of corium has been molten, the arc power is reduced and the cathode is withdrawn. The furnace is then tilted so that the melt pours out in the test section. The plasma arc is kept operating during the pouring operation, in order to maintain the melt temperature.

2.2. Test sections

Up to now, two major configurations have been used for the VULCANO experiments. In the VULCANO-E configuration, which is mainly devoted to the study of corium spreading, the test section consists of a spreading plane. It can be made of refractory bricks (e.g. zirconia or magnesia), of a steel plate or concrete. Two geometries have, up to now, been used: spreading in an open square or in a 19° angular sector (Fig. 2). The spreading section limits are materialized by refractory magnesia bricks.

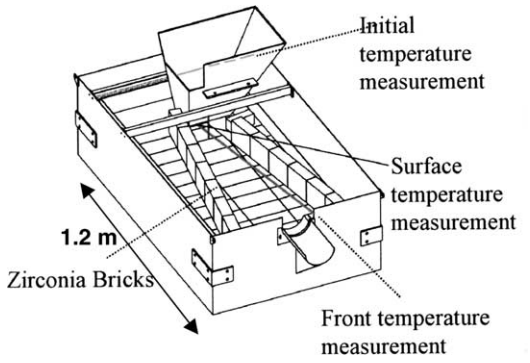

Fig. 2. Total 19° angular sector test section with pyrometer locations.

In a second configuration (VULCANO-P) devoted to the physico-chemistry and its influence on corium long-term behavior (Journeau et al., 1999a, 2001a), the melt is poured in a cylindrical crucible made of refractory material with a possible lining of sacrificial material. Induction heating is used to simulate the corium radiological decay heat (Jégou et al., 2001) which is necessary for these long duration experiments whereas it was not useful for spreading tests which deal with transient flows (of less than 1 min). This paper is devoted to the spreading configuration (VULCANO-E).

2.3. Instrumentation

The test section is mounted on a weighing scale in order to measure the pouring flow rate.

Temperature measurements are performed by thermocouples (K, N, S and B or C—tungsten–rhenium—types), bichromatic pyrometers and infrared thermography (Cognet et al., 1995).

Spreading progression and front velocity are measured with geometrically calibrated cameras (Journeau et al., 1998) and compared with the temperature rise of surface thermocouples. The geometrical calibration (see Fig. 3) is obtained by positioning a checkerboard on the spreading section and correlating the pixel position with the vertices co-ordinates.

The infrared camera is in situ cross-calibrated (Cognet et al., 1995) with a bichromatic pyrometer, the aiming point of which is positioned on the thermographic images. The least square fitted correlation is then used to convert the thermographic images in temperature maps. This calibration takes into account simultaneously the intrinsic calibration of the device and the corium surface emissivity in the considered infrared bandwidth (Fig. 4).

2.4. Post-mortem analyses

After the test, the cooled and solidified corium is examined. Its shape is measured (e.g. Fig. 5) and samples are taken for chemical and material post-mortem analyses (e.g. Journeau et al., 2001a,b).

Chemical analyses are made on crushed samples using an X-ray fluorescence (XRF) analyzer. X-ray diffraction (XRD) analyses are performed for phase identification. Resin-wrapped samples are observed using optical microscopes and a scanning electron microscope (SEM). Local composition is estimated with an energy dispersive spectrometry (EDS) microanalysis probe. For the spreading experiments, the element

Fig. 3. Checkerboard used to calibrate the “fish-eye” camera before test VE-U1.

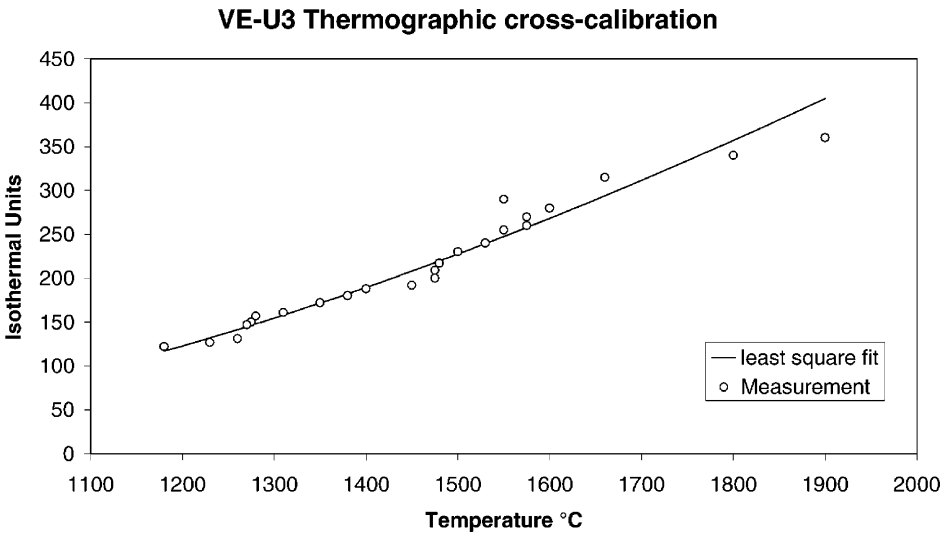

Fig. 4. Cross-calibration of infrared thermography and bichromatic pyrometry. Isothermal units are arbitrary units proportional to the luminance of the observed object.

composition is relatively constant over the spread volume, but there are important variations against height in terms of compositions and microstructures.

The chemical results are compared with thermodynamic computations which have been carried out using THERMODATA's GEMINI2 software and the TDBCR databases (Chevalier et al., 1997). The main findings of these analyses will be reported in Section 4.3.

3. The spreading tests

Due to the practical and regulatory constraints linked to the use of depleted uranium dioxide, some tests have been performed with non-radioactive high-temperature corium simulants in order to prepare the tests with prototypic corium. These tests are generally interesting as a reference to assess uranium-related material effects. A first series of tests have been made with zirconia–alumina mixtures in order to reach the desired temperature range. In a second series of simulant material tests, hafnia (HfO_2) simulated urania (UO_2). It has been chosen because of its high density, high melting point and its physico-chemical closeness to urania. Nevertheless, the urania–zirconia and hafnia–zirconia pseudo-binary are not totally equivalent (Fig. 6): there is an azeotropic point between liquid urania and zirconia (Cohen and Schaner, 1963) whereas there is no azeotrope for hafnia and zirconia (Ruh et al., 1968).

After these high-temperature simulant material tests, five spreading tests with prototypic corium have been performed and will be described in Sections 3.4–3.8 (and synthesized in Table 3).

3.1. High-temperature simulant tests on 2D sections

Two tests have been performed with zirconia–alumina melts that were spread on a square test section with an inlet smaller than the square section side. During test VR-18, which was the first high-temperature melt spreading at the VULCANO facility on 23 May 1996, 6.5 kg of 55 wt.% zirconia, 45 wt.% alumina spread over a 450 mm × 525 mm spreading section. Fig. 7 shows the dissymmetric final shape of the spread.

During the next test, VR-19, 23 kg of a zirconia–31 wt.% alumina mixture totally filled the 0.24 m^2 spreading area. Due to the spurious presence of thick fumes, it had not been possible to visualize flow progression, but spreading velocities between 15 and 30 cm/s had been measured by surface thermocouples. These tests showed for binary mixtures a good spreadability leading to a small final melt thickness.

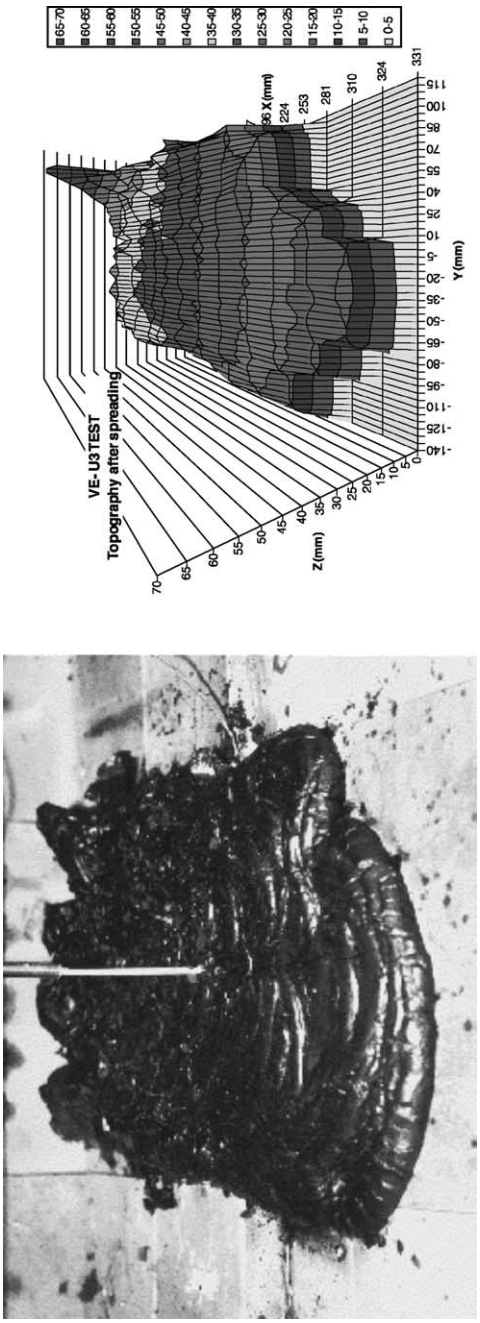

Fig. 5. Left: View of the VE-U3 corium spread (after dismounting the spreading section walls). Right: Measured shape (481 surveying points).

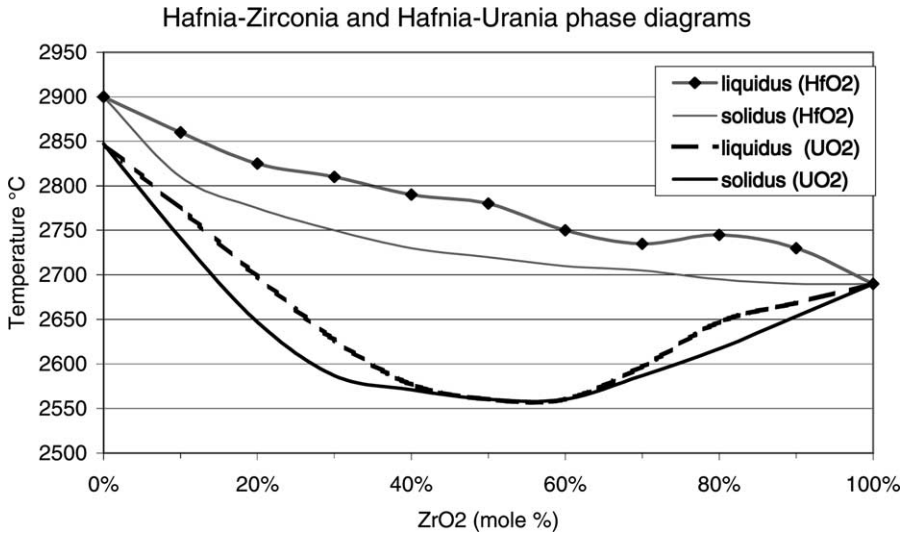

Fig. 6. Liquidus and solidus temperatures for the HfO_2–ZrO_2 (Ruh et al., 1968) and UO_2–ZrO_2 (Cohen and Schaner, 1963) pseudobinaries.

3.2. High-temperature simulant tests on 19° angular sector

Five tests have been performed with simulant materials on a 19° angular sector, in order to model, with limited masses, axisymmetric spreading. In this geometry, the inlet covers the totality of the test section smaller side (see Fig. 2). The simulant melts represented corium–concrete mixtures by replacing mole-wise uranium by hafnium. In these tests, the melt presented only a few surface cracks and very little porosity; post-mortem, the final porosity corresponded only to shrinkage (the density difference between liquid and solid states). The main characteristics of these tests are reported in Table 1.

3.3. High-temperature simulant test with metal/oxide melt

An experiment (test VE-06) has been performed in which metallic iron has been added to the oxidic melt. The spread composition was, in mass percentages, around 52% HfO_2, 14% ZrO_2, 27% Fe_2SiO_4, 2% CaO, 5% Fe, simulating the mixture of 71% of a mixed metal/oxide corium with 29% of ferrosiliceous concrete.

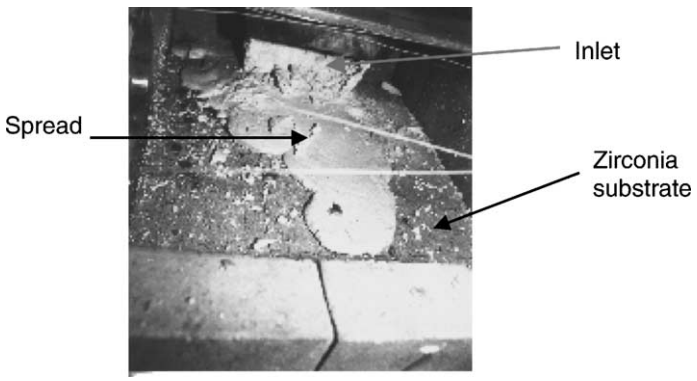

Fig. 7. Post-mortem view of the VR-18 spread (unbounded 2D spreading).

Table 1
Physical and chemical characteristics of simulant spreading tests on $\theta = 19^\circ$ angular sector

Test	Composition (wt.%)	Mass (kg)	Flow rate (l/s)	Pouring temperature (°C)	Liquidus–solidus (°C)	Main results
VE-01	50% HfO_2, 10% ZrO_2, 34% $Al_6Si_2O_{13}$, 6% $Al_2CaSi_2O_8$	12	0.1 discontinuous	1800	2130–1350	Small spreading: 22 cm, thickness 40 mm
VE-02	58% HfO_2, 10% ZrO_2, 31% $Al_6Si_2O_{13}$, 1% CaO	21	0.1 discontinuous	2000	2230–1530	Accumulation, thickness 40–100 mm
VE-03	40% HfO_2, 5% ZrO_2 39% Fe_2SiO_4, 16% Fe_3O_4	15	0.1 discontinuous	1800	1830–1070	Spreading length 30 cm, thickness at front 20 mm
VE-04	61% HfO_2, 11% ZrO_2, 21% Fe_2SiO_4, 4% Al_2O_3, 3% CaO	12	0.7 discontinuous	2000	2130–1050	Accumulation, no spreading
VE-07	33% HfO_2, 22% ZrO_2, 22% SiO_2, 22% FeO, 1% CaO	17	0.5 discontinuous	1975	2100–1000	Spreading length 55 cm, high compactness homogeneous structure

Uncertainties are around ±70 °C for the temperatures and around ±20% for pouring rates.

A total of 34 kg of melt were spread over a final length of 45 cm. The molten iron remained in droplets which formed sort of an emulsion with the oxidic liquid and did not sediment although the temperature remained above the iron melting point for 3 min and the oxides were significantly less dense than iron. Fig. 8 presents a cut view of the spread: iron droplets are visible which are covered by a thin oxidation layer. So there were no macrosegregation during this spreading test. It is expected that spreading and sedimentation will occur subsequently in the reactor case, at least if the fraction of metal is low. (In the reactor case, decay heat will delay the oxidic phase solidification, allowing sedimentation in a latter stage.)

3.4. VE-U1

The first spreading experiment with prototypical material, VE-U1, was performed in the VULCANO facility on 2 December 1997. The corium composition (in mass percentages: 44% UO_2, 23% ZrO_2, 21% SiO_2, 12% FeO_x) was prototypic of corium discharge from the EPR reactor pit after ablation of sacrificial ferrosiliceous concrete. The solidification range of this mixture is of about 900 °C with a liquidus temperature

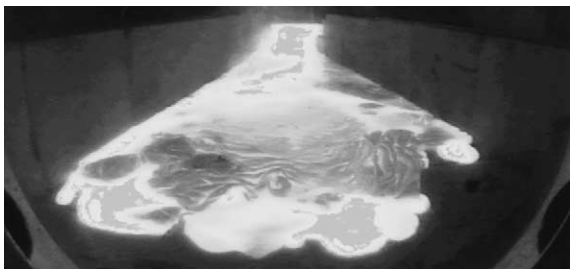

Fig. 9. Front view of the VE-U1 spread during the experiment (taken with the camera calibrated in Fig. 3).

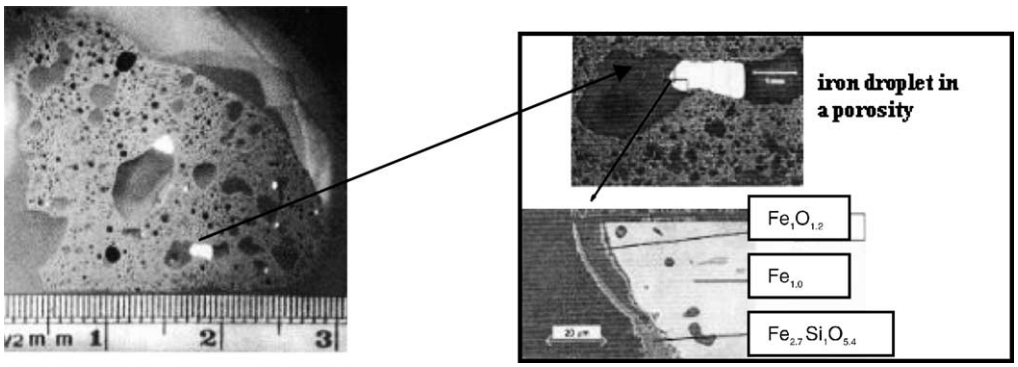

Fig. 8. VE-06: Cut of the melt front.

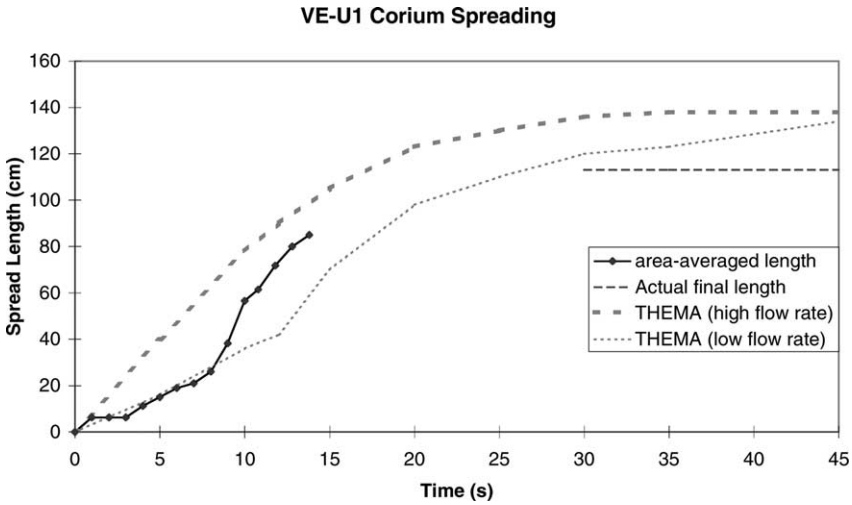

Fig. 10. Progression of corium length as measured from the video images, compared to the values calculated by THEMA spreading code (see Section 4.2). The measurment has been interrupted after 15 s when part of the spread was out of the video image field.

of 1975 °C, 38.8 kg of corium, at an initial temperature of 1820 ± 100 °C, spread over 1.2 m. Fig. 9 shows a view of the spread, taken when the front was at 0.9 m from inlet. The flow length evolution (Fig. 10) has been obtained from the analysis of video images and is consistent with the time of passage recorded on surface thermocouples. It gives a maximum front velocity of 0.2 m/s. The corium surface temperature has been measured by pyrometers (Fig. 11). Substrate temperature has also been monitored by thermocouples at the interface and 10 mm deep.

Thermograms for two axial positions (20 and 133 mm downstream of inlet) are shown on Fig. 12. The a priori puzzling fact that the upstream sensor

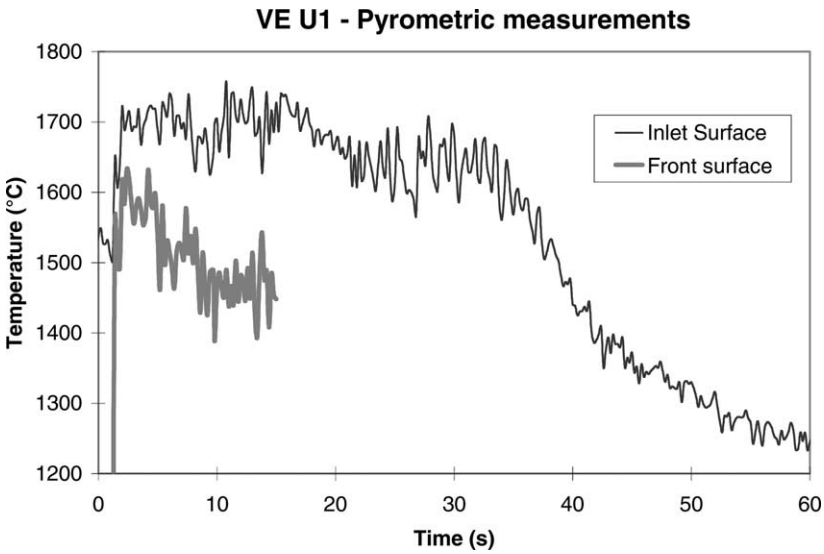

Fig. 11. VE-U1 surface temperature measurements at the inlet surface and at the front (see Fig. 2 for pyrometer locations). The mirror used for front temperature measurements was reached by corium flow at $t = 15$ s.

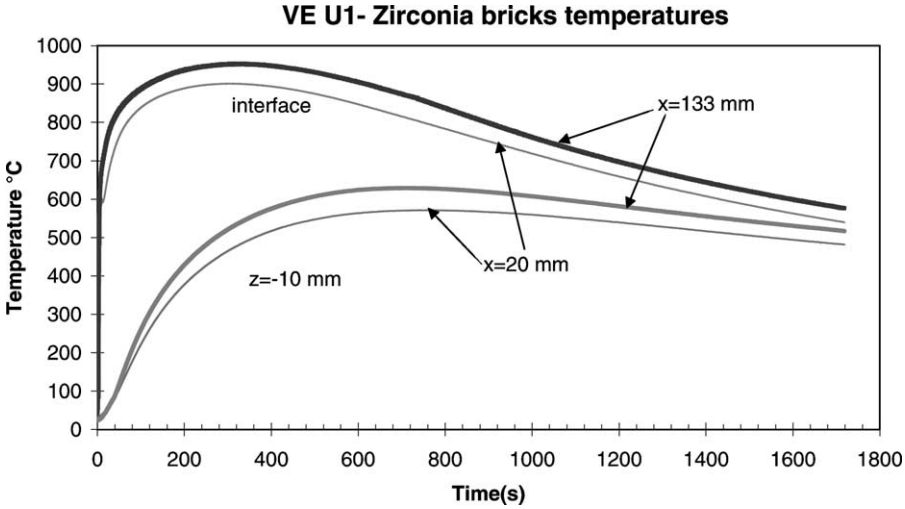

Fig. 12. VE-U1: Evolution of the brick temperature.

raises later than the downstream one and to a lower temperature is attributed to the presence of a small early splash of corium right above this thermocouple (as confirmed by the video) which had cooled down before being covered by the spread and acted as a thermal shield.

Post-mortem observations showed the presence of large macroporosities in the spread, estimated at about 30 vol.% There has been little interaction between corium and the sintered-zirconia bricks.

3.5. VE-U3

The VE-U3 test used a mixture with a smaller concrete content, having the following composition, in mass percentage: 63% UO_2, 22% ZrO_2, 8% SiO_2, 7% FeO, i.e. being richer in UO_2—and thus having a 150 °C higher liquidus temperature—than VE-U1 corium. A total of 15.6 kg of corium, poured at an initial temperature of 2130 ± 60 °C, which is below the liquidus temperature (~2375 °C according to a GEMINI2 calculation using TDBCR991) with a flow rate of 0.3 l/s, have spread over 33 cm with an average height of 32 mm. Fig. 5 presents a view of the spread after the test and its shape as measured post-mortem. The corium temperature has been monitored by three pyrometers (see positions in Fig. 2) and a type-C tungsten–rhenium thermocouple; the temperature evolution is shown in Fig. 13. The delay between pyrometer and thermocouple readings is due to the

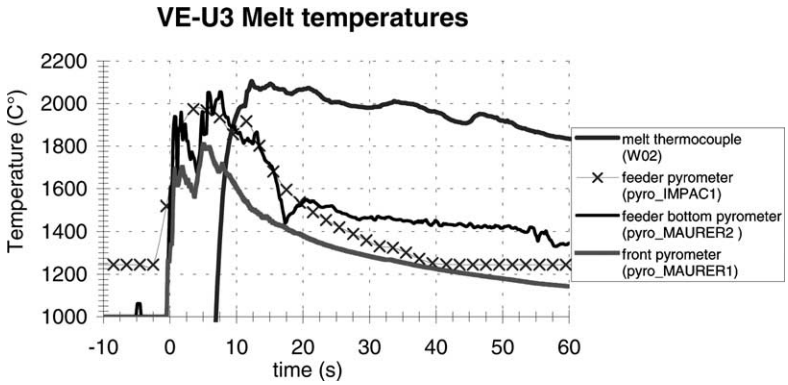

Fig. 13. Evolution of corium melt temperature during test VE-U3 from pyrometer and in-corium type-C thermocouple.

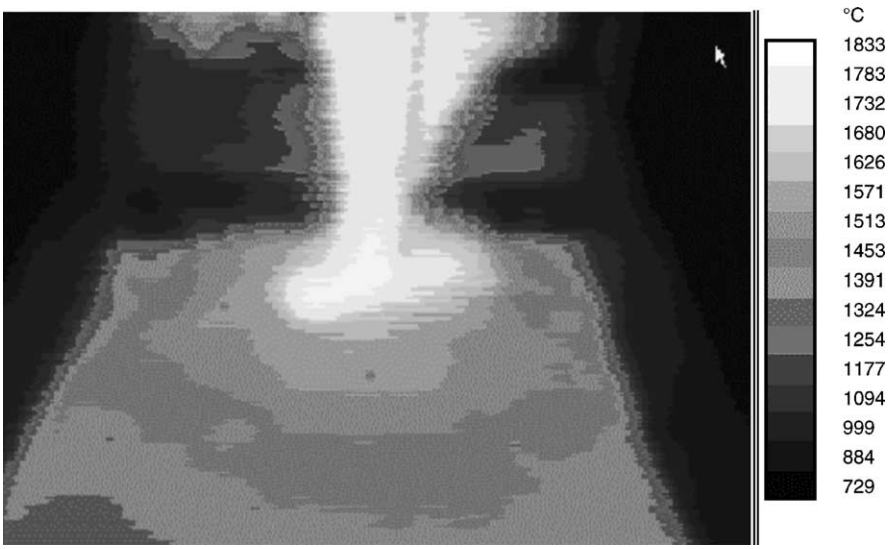

Fig. 14. Infrared thermography view of the corium first flow in test VE-U5.

necessary time to heat the sensor and the corium crust that formed at contact (Journeau et al., 1999b).

In this test, the observed porosity was small, corresponding to shrinkage.

The main conclusion of this test is that although pouring conditions (initial melt temperature 250 °C below liquidus and low flow rate) were unfavorable, such a corium mixture effectively spread, certainly because of its large solidus–liquidus temperature range of 1200 °C.

3.6. VE-U5

In this test, two successive spreading phases were realized with a corium of the following initial composition: 46 wt.% UO_2, 10 wt.% ZrO_2, 24 wt.% FeO, 20 wt.% SiO_2. A first part of the corium flow was poured on the steel spreading section (see thermographic view in Fig. 14) while a second part was maintained temporarily in a crucible, where an exothermic reaction with metallic zirconium provided chemical heating. When the crucible steel-door melted, a second flow occurred which mixed with the already-stopped first spread and induced a subsequent flow underneath the first immobilized corium surface and a rupture of the first front (visible in bright on Fig. 15). In total, 36 kg were spread at a mass flow rate of 2 kg/s (0.5 l/s) with an initial temperature around 1830 °C.

Fig. 16 presents the temperature measured at the iron spreading plane surface. It never exceeded 850 °C. It also clearly shows the effect of the subsequent spreading which did not increase the temperature of the plate already covered by the melt and induced a relatively weak increase of temperature of the newly covered part of the iron plate.

Fig. 15. VE-U5 corium spread over a steel plate (the molten metallic gate of the crucible is visible as a bright spot in the upstream of the flow).

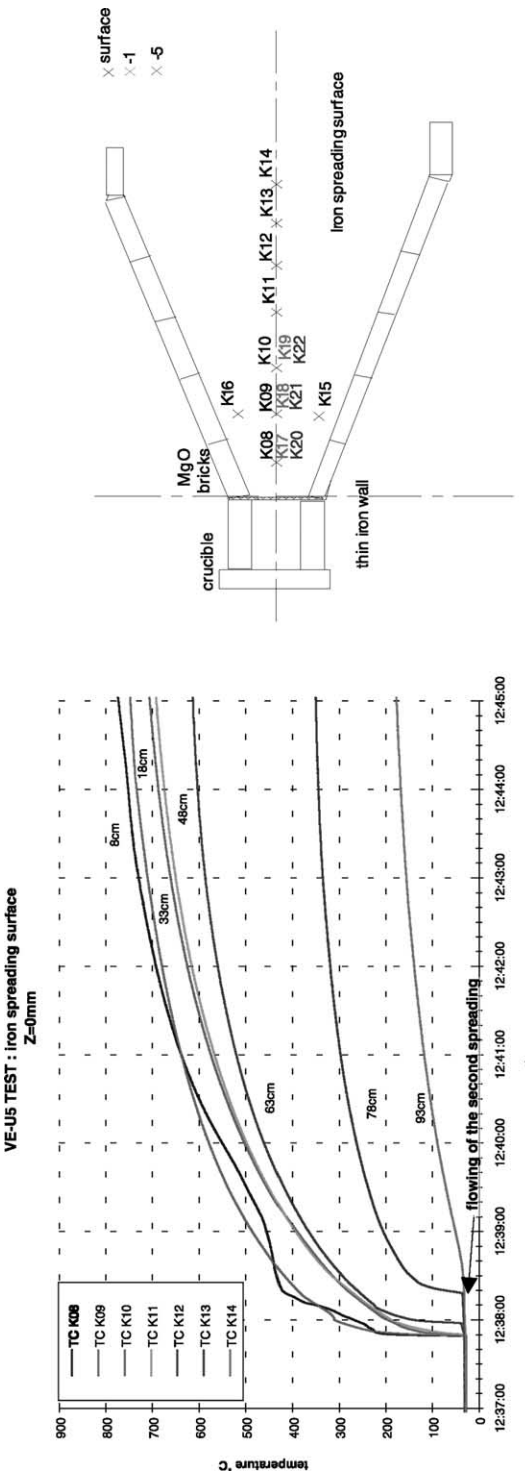

Fig. 16. Left: Temperature evolution at the iron plate surface. Right: Thermocouple location in the iron spreading plate.

This test showed the ability of corium–concrete mixtures with large solidification ranges (here 1100–1940 °C) to progress even when a second load is poured after the initial progression had stopped.

3.7. VE-U7

VULCANO experiment VE-U7 has been dedicated to the study of spreading over ceramic and concrete substrates. The concrete has been made of CEM I 32.5 R concrete mixed with silica granulates, corresponding to a composition that had been previously studied on KAJET test KJ04 (Steinwarz et al., 2002). The reference channel was made of dense inert bricks of fused zirconia.

The corium had the following average composition, in mass percentage, 61 wt.% UO_2, 30 wt.% ZrO_2, 3 wt.% FeO, 2 wt.% Fe, 2 wt.% SiO_2, 2 wt.% $CaSiO_3$, 0.6 wt.% CaO, 0.4 wt.% Al_2O_3, which is close to a corium composition that had been computed by Nie (2000) for the oxidic part of the corium flowing out of the EPR gate.

About 50 kg of corium have been poured, 40 kg of which reached the spreading section with a flow rate of 3 kg/s. The initial temperature at the spreading section entrance was 2175 ± 75 °C for a liquidus temperature of 2375 °C and a solidus of 1000 °C.

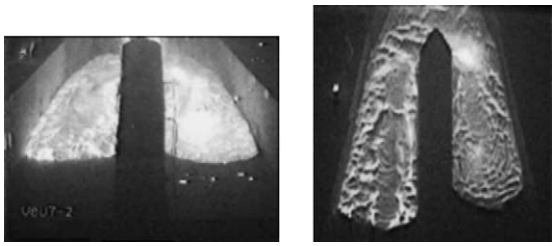

Fig. 17. Front and top view of the VE-U7 corium spreading. Concrete is on the right hand side, ceramic on the left.

The section has been designed and aligned so that the hydrodynamic flow was equally distributed between the two channels. A total of 12 kg flowed to the channel on concrete, 14 kg on the ceramic, the remainder staying in the distribution pool at the upstream of the test section (see Fig. 17). The flow over concrete stopped at a slightly smaller distance and its front is much steeper than on ceramic (see Fig. 18). Some hot spots and splashes have been observed on the concrete side. These eruptions lasted for 20 s after the stop of corium progression. The temperature evolution has been monitored in both substrates (Figs. 19 and 20).

Numerous fumes have been produced both over concrete and ceramic, even though the only external source of gas was the concrete free and bounded water. High porosities were observed in the two spreads

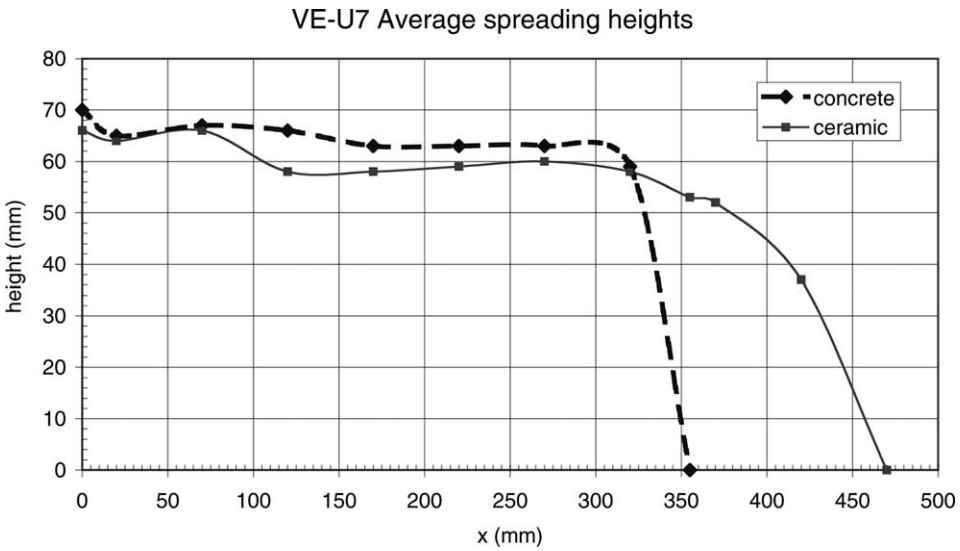

Fig. 18. Post-mortem measurement of the spread profile for VE-U7 two channels.

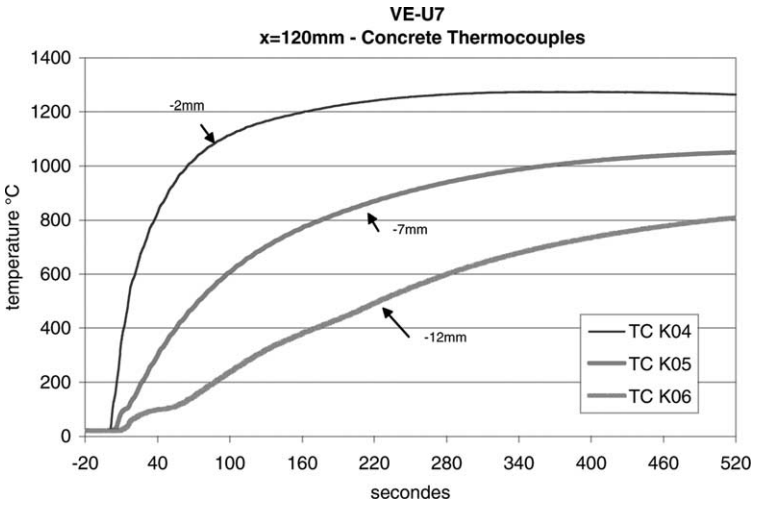

Fig. 19. VE-U7: Concrete temperature at 12 cm from origin and at depths of 2, 7 and 12 mm.

(see Fig. 21), which had, post-mortem, the same specific mass within measurement uncertainties: $5000 \pm 200\ kg/m^3$.

The concrete substrate was slightly attacked on a few millimeters. Mortar has been more attacked than surrounding silica aggregates.

3.8. VE-U8

In test VE-U8, in-vessel corium (theoretical composition: 80 wt.% UO_2–20 wt.% ZrO_2) has been spread at ~2660 °C onto a 20 wt.% lime–80 wt.% silica concrete for about 40 cm. For this configuration the liquidus–solidus range is small—less than 50 °C according to Cohen and Schaner (1963)—and lies between 2600 and 2700 °C. In other words, the uncertainty on temperature measurements is of the order of magnitude of the solidification range.

Fig. 22 presents the shape of the 30 kg spread. Cracks formation has been surveyed during the cooling phase and the effect of the gaseous products of the corium–concrete interaction has been observed.

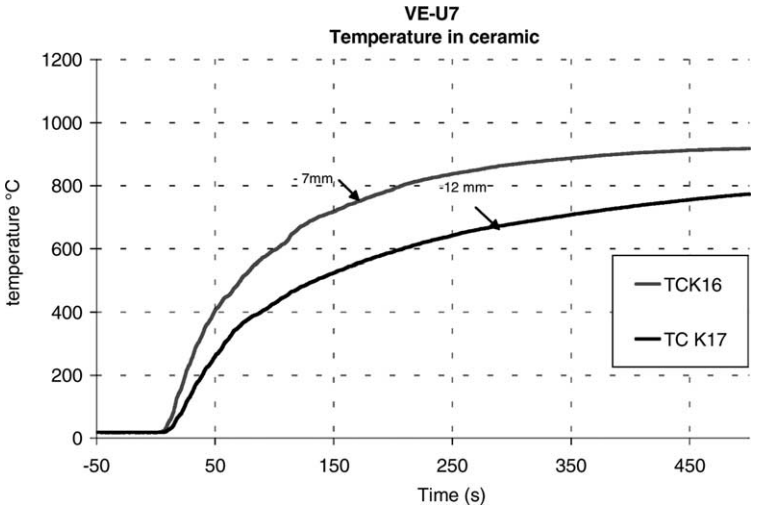

Fig. 20. VE-U7: Ceramic temperature at 12 cm from origin and at depths of 7 and 12 mm.

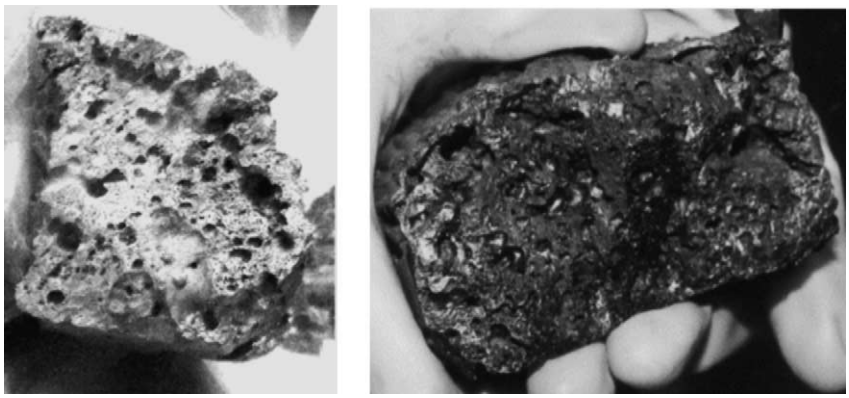

Fig. 21. Cut views of VE-U7 spread over dense zirconia (left) and siliceous concrete (right).

Fig. 22. Post-mortem view of the VE-U8 UO_2–ZrO_2 in-vessel corium over a silica—20 wt.% limestone concrete substrate.

With this composition, and contrary to what has been observed in previous tests with corium–concrete mixtures, a solid crust is rapidly formed at the upper surface during spreading which can be broken by sparging gas pressure. Although the flow rate was higher (1 l/s) than for previous tests, the final spreading length was not specially large.

Even though there were no sustained heating, up to 2 cm of concrete have been ablated (see Fig. 23). Fig. 24 presents the evolution of concrete temperature during the interaction. The concrete is heated to much higher temperatures than during test VE-U7 and at a much steeper rate. Thermodynamic computations with TDBCR001 indicate that this concrete reaches 50 vol.% of liquid at a temperature around 1300–1400 °C. At this measurement point (12 cm

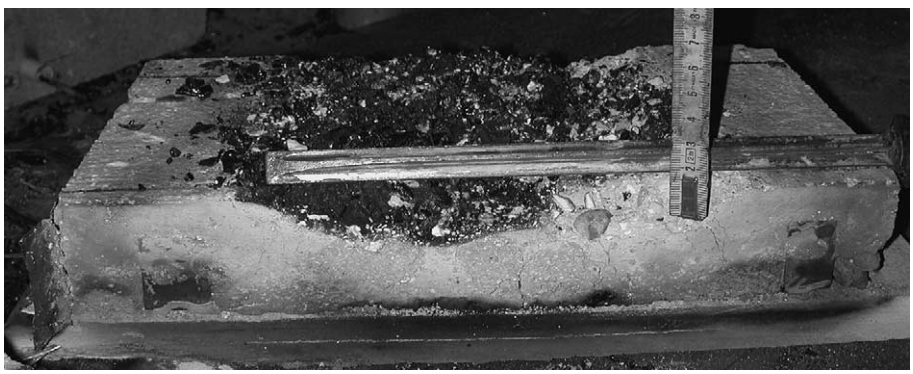

Fig. 23. Silica: 20 wt.% limestone concrete ablated by UO_2–ZrO_2 corium during test VE-U8. The maximum ablation depth is of 2 cm.

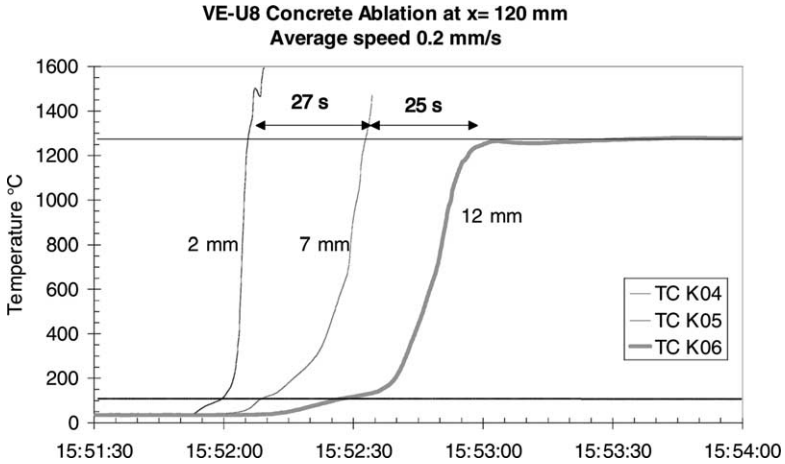

Fig. 24. VE-U8: Temperature evolution inside the concrete substrate.

Table 2
Estimation of gas superficial velocity during test VE-U8

	Free H_2O	Bound H_2O	CO_2
Temperature (°C)	100	~500	~800
Progression of isotherm (mm/s; from TC readings)	0.37	0.24	0.2
Quantity in concrete (mol/m^3)	3600	3600	2200
Molar flow rate (mol/m^2/s)	1.34	0.86	0.47
Superficial velocity at 1400 °C (m/s; 1 mol = 127 l)	0.17	0.11	0.05

The total gas superficial velocity is of 0.33 m/s.

Table 3
Physical and chemical characteristics of prototypic corium spreading tests

Test	Composition (wt.%)	Mass (kg)	Flow rate (l/s)	Pouring temperature (°C)	Liquidus–solidus (°C)	Main results
VE-U1	44% UO_2, 23% ZrO_2, 21% SiO_2, 12% FeO_x	38.8	0.6	1820	1975–1030	Spreading over 1.2 m, several tongues, large voids
VE-U3	63% UO_2, 22% ZrO_2, 8% SiO_2, 7% FeO	15.6	0.3	2130	2375–1050	Spreading over 33 cm, small porosity
VE-U5	46% UO_2, 10 wt.% ZrO_2, 24 wt.% FeO, 20% SiO_2 + zirconium metal	36	0.5	1830	1940–1100	Successive spreads
VE-U7	61 wt.% UO_2, 30 wt.% ZrO_2, 3 wt.% FeO, 2 wt.% Fe, 2 wt.% SiO_2, 2 wt.% $CaSiO_3$, 0.6 wt.% CaO, 0.4 wt.% Al_2O_3	26	0.7 l/s divided in two channels	2175	2375–1000	Parallel flows on ceramic and siliceous concrete, similar length (36/45 cm) and porosity for both substrates
VE-U8	80% UO_2, 20% ZrO_2	30	1 l/s	2660	2650–2610	40 cm length, solid crusts on surface 2 cm ablation of 80% silica–20% limestone concrete

Uncertainties are around ±70 K for the temperatures and around ±20% for pouring rates.

downstream of the origin), the concrete reached temperatures over 1300 °C on 12 mm. The solidus front velocity was of about 0.2 mm/s. From the progression of the isotherms, it is also possible to estimate the gas superficial velocities from the progression of the 100 °C (free water), 500 °C (bound water) and 800 °C (carbon dioxide) isotherms, assuming that corresponding volumes of gases are liberated when these temperature are reached. The total gas superficial velocity is estimated at about 0.3 m/s (Table 2). Further analysis of this test is in progress.

3.9. Summary table of prototypic corium tests

Table 3 summarizes the five spreading tests performed with prototypic corium in the VULCANO facility. The initial corium temperatures range from 1700 to 2700 °C. It must be noted that although the maximum mass on the spreading section was of 39 kg, up to 65 kg of corium have been poured out of the furnace, the remainder being lost in the devices dedicated to flow stabilization.

4. Major results

These tests have shown that spreading of corium–concrete mixtures is quite efficient, even at low flow rates, with inlet temperatures below the liquidus and with composition containing up to 22 wt.% of silica (i.e. viscous liquids). It must be stressed that the absence of sustained heating in these tests is conservative since decay heat will (slightly) delay the solidification process. They also enabled us to validate and improve our modeling of the rapid cooling processes taking place during the spreading transient.

4.1. Spreading behavior

Two different phenomena have been observed depending on the presence of concrete decomposition products in the spread mixture.

For in-vessel corium (VE-U8), as in FARO spreading tests (Tromm et al., 2000), the corium surface formed rigid solid crusts. These crust were seen rafting over the liquid and broke at several occurrences, leading to a stop and go progression. The corium surface was quite rough.

For corium–concrete mixtures, there is rather a smooth viscous skin on the corium surface. This surface skin is generally folded (e.g. Figs. 5 and 9) as in ropy pahoehoe lavas (Cas and Wright, 1988). It has been shown (Journeau et al., 1999a, 2001a) that these folds are due to instabilities caused by the rapid variations of viscosity with depth at the upper boundary layer. The progression at the front is similar to that of half-track motion, the upper surface drifting at a velocity higher than the front velocity.

The major effect of concrete decomposition products is that it enlarges substantially the solidus–liquidus interval from 50 to 100 °C for (U, Zr)O_2 mixtures (such as in VE-U8 test) to more than 1000 °C (as in VE-U7). The amount of heat to extract before the crust is fully solid is more than twice for corium–concrete mixtures than for urania–zirconia corium. Thus, during spreading of corium–concrete mixtures, the surface remains viscoplastic while it is completely solidified for (U, Zr)O_2 mixtures. It is believed that the good spreadability of corium–concrete mixtures, even if the initial temperature was largely below liquidus, is due to the existence of a large solidification range.

4.2. Validation of spreading models and codes

One of the major objectives of this series of tests was to validate spreading models and codes for severe accident management.

4.2.1. Dinh et al. (2000) simplified model

Dinh et al. (2000) have proposed a simplified model based on a scaling approach. They assume that corium flows as an isothermal viscid hydrodynamic fluid for the time needed to cool its front down to an immobilization temperature. A characteristic spreading velocity U can be estimated with Huppert (1982) model for axisymmetric gravity-viscous spreading with constant volume flow rate and viscosity:

$$U = \left(\frac{gG^3}{3\nu}\right)^{1/8} t^{1/2}$$

where G is the volume flow rate, ν the kinematic viscosity and t a characteristic time of corium discharge.

The characteristic time for solidification is estimated as the time necessary to reach the temperature of an effective solidification T_{sold} considering heat

Table 4
Front surface temperature at immobilization for the tests were this information was recorded

	Test					
	VE-04	VE-07	VE-U1[a]	VE-U3	VE-U7	VE-U8
Stopping temperature (°C)	1700–1850	1450–1600	<1400–1550	1400–1550	1500–1650	2300–2400
Solid volume fraction (vol.%)	60–75	60–70	>60–70	70–80	65–75	100

[a] VE-U1 measurement was interrupted when moving corium covered the mirror.

losses by radiation (at the inlet temperature) and convection (with the $Nu = 0.0023\,Pe$ correlation (Dinh et al., 1997) for heat transfer over a rough crust). Physically, it corresponds to the time at which a characteristic element of the front is immobilized, assuming that it will effectively stop the corium progression and determine its length.

The front temperature at immobilization has been measured on several tests using a pyrometer aiming horizontally thanks to a mirror. These front immobilization temperatures (Table 4) correspond in most cases to solid fractions of about 70 vol.% for corium–concrete mixtures and to values below solidus in case of in-vessel corium. It must be noted that these temperatures are measured at the front surface while there are steep gradients in the thermal boundary layer (Journeau et al., 1999a, 2001a). Actually, the characteristic front element is at an average temperature higher than the front surface. In the absence of more precise data, the immovability temperature has been set arbitrarily as the temperature corresponding to the average of the enthalpy at the liquidus and solidus temperature. This approach explains the good spreadability of corium–concrete mixtures since, for instance, 1.5 times more enthalpy must be removed from VE-U1 ex-vessel composition to reach this immovability criterion than for VE-U8 in-vessel corium composition.

For Dinh et al. (2000) model, the final average height order of magnitude δ_s is given, for 1D spreading by the following expression:

$$\delta_s = \max\left[\delta_{cap}, \frac{V_{tot}^{3/4}[q_{rad} + q_{conv} - q_v\delta_{cap}]^{1/2}}{G^{7/16}(g/3\nu)^{1/16}\rho_m^{1/2}(H(T_m) - H(T_{sold}))^{1/2}}\right]$$

in which δ_{cap} is the capillary limit; V_{tot} the total spread volume; q_{rad}, q_{conv} and q_v, respectively the radiated, convected and volumic heats; ρ_m the melt density; H the enthalpy; and T_m is the melt initial temperature.

This approximate method gives, for the VULCANO-E test, the order of magnitude of the final corium height (values between 0.5 and 2 times the experimental value). For example, Fig. 25 presents the calculated spreading length for various values of initial corium temperature and flow rate corresponding to VE-U1 configuration. This scaling law approach is consistent with the experimental results.

4.2.2. THEMA code

Eberlé (1997) has developed the THEMA software that integrates the conservation of mass, energy and momentum over verticals of the flow (Spindler et al., 2000). The melt is either homogeneous or composed of two possible stratified components (mixture of metals and mixture of oxides).

A single momentum equation is considered under the shallow water assumption, whereas two energy equations are used, one for the metallic and one for the oxidic component. Furthermore, several mass balance equations are used, one for each material of the two metallic and oxidic components. The melt model is based on 2D balance equations as a result of the integration over the melt thickness of the 3D equations. As a consequence, specific constitutive laws in terms of depth averaged variables (velocity, temperature) are needed: wall shear stress for the momentum equation, heat transfer coefficients for the energy equation.

Crust formation at the bottom and at the surface of the melt are taken into account with specific models. These models are based on energy balance across the crust and at the melt-crust interface.

For non-congruently melting materials, the melt mean temperature may have a value between the

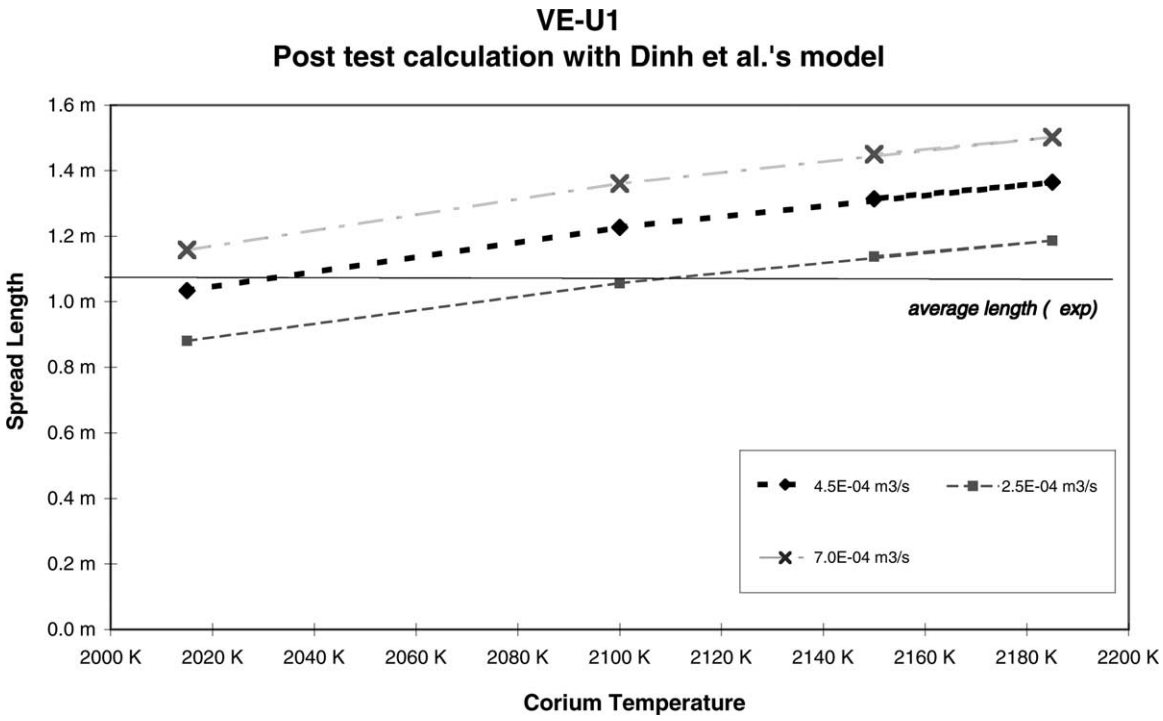

Fig. 25. Effect of corium initial temperature and flow rate on the computed spread length Dinh et al. (1997) model: VE-U1 data.

solidus and liquidus temperatures. Viscosity models are included in the code, giving a sharp increase of the viscosity when the temperature decreases, and as a consequence the stopping of the spreading. The other mechanisms of front stopping are the surface tension and the crust formation itself, reducing the melt mass.

The numerical integration of the finite difference set of equations uses a semi-implicit method with a Newton–Raphson iteration procedure. A second order discretization in space is used to get a better accuracy of the melt front progression. The temperature field in the solid substrate is solved apart from the melt equations, with a 3D meshing using the alternate direction method for solving the conduction equation in a solid, including ablation.

As far as wall shear stress is concerned, a classical law is used, based on a Reynolds number with the hydraulic diameter equal to four times the melt height. Correlations for heat transfer coefficients, valid either for Prandtl number *Pr* of order of magnitude 1 or small Prandtl numbers (Duchatelle and Vautrey, 1964), are used to compute heat transfer between the melt and the crust, or if no crust, between the melt and the upper surface and between the melt and the substrate. The heat transfer between the upper surface and the surroundings corresponds to radiation, with the emissivity of the spreading surface and the emissivity of the surroundings given in data.

This code has been satisfactorily validated against VULCANO spreading experiments. For example, Fig. 10 presents the spreading-length evolution computed for VE-U1 considering two hypotheses for the evolution of inlet flow (which is indirectly known since the mass in the inlet is not distinguished from that on the spreading section). Currently, the main obstacle to a precise validation is due to the large uncertainties still present on the corium physical properties. They can lead to computed final spreading lengths between 0.6 and 2 m for VE-U1—for an experimental average value of 1.13 m.

An uncertainty analysis made on 255 different data sets within the uncertainty range for VE-U1 spreading test pointed out (see Fig. 26) that the prevailing

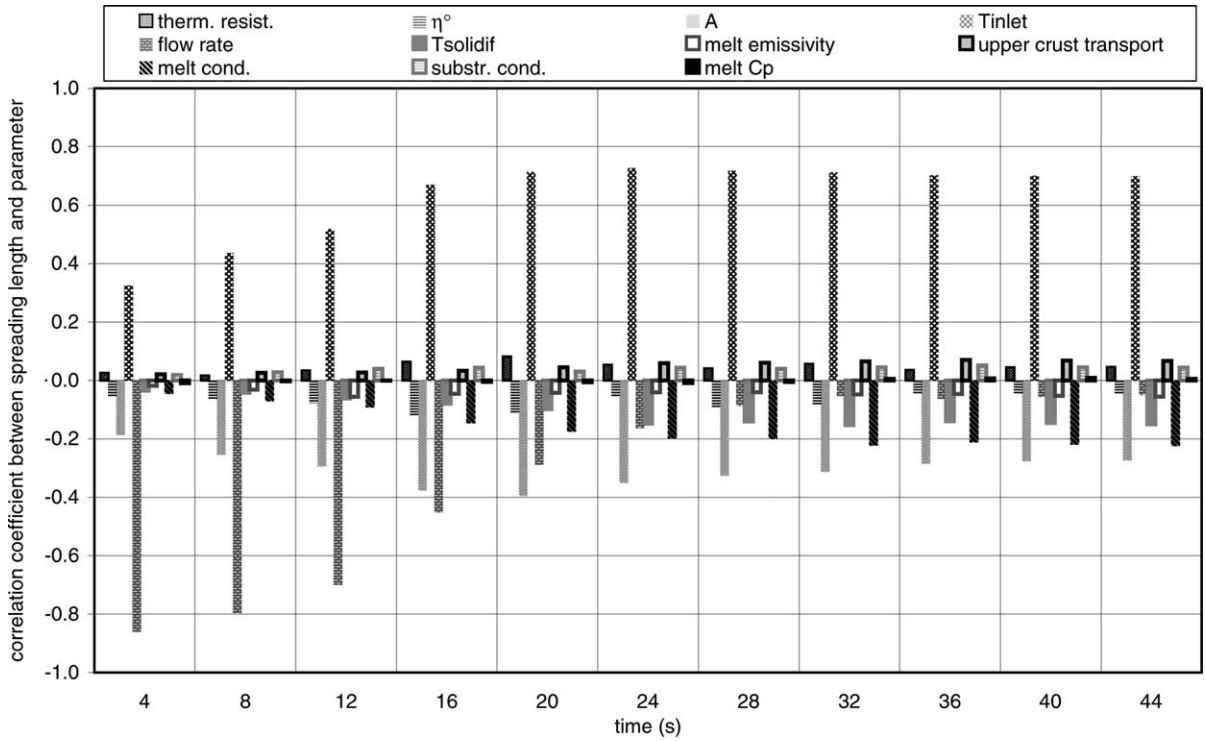

Fig. 26. Correlation coefficients between the spreading lengths calculated for the VE-U1 test with THEMA V2.3mod6 and the following parameters: thermal resistivity; η^0 and A in the exponential fit for viscosity ($\eta = \eta^0 \exp[A(T_{\text{liquidus}} - T)]$); inlet temperature; flow rate; solidification temperature; melt emissivity; upper crust transport (i.e. crust velocity to melt velocity); melt thermal conductivity; substrate thermal conductivity; melt heat capacity.

parameters for the spreading lengths are the liquidus temperature, the exponential parameter A describing the viscosity temperature law (the viscosity, estimated as described later in Section 4.4, is fit, for computational simplicity by an exponential law $\eta = \eta^0 \exp[A(T_{\text{liquidus}} - T)]$), the initial melt temperature, the melt flow rate and the melt conductivity. The less influent parameters are the surrounding temperature, the corium emissivity and the substratum conductivity.

Concerning the substrate temperature, the substrate surface temperature evolution depends mainly on the thermal resistance, the melt conductivity, the initial melt temperature while the temperature evolution, 1 cm under the surface, mainly depends on the melt and substratum conductivities, the thermal resistance (mainly at the end of the spreading process), the melt flow rate (mainly at the beginning of the spreading process) and the initial melt temperature.

A 2D horizontal mesh was used to calculate the VE-U7 test. Here also, there are large uncertainty bars on the inputs. The following set of input parameters gives a satisfactory fit between experiment and calculations: inlet temperature 2227 °C; viscosity law $\eta = 0.0260\,\mathrm{e}^{-0.0300^{(T-T_{\text{liquidus}})}}$ Pa s; thermal contact resistances of 1.2×10^{-3} and 5.4×10^{-3} K m^2/W, respectively, for concrete and ceramic substrate.

In parallel to prototypic corium tests, the code has been validated with low temperature simulants, the properties of which are well known (Spindler et al., 2000). Therefore, there are now sufficient experimental validations of this code.

4.2.3. Other spreading codes

The 1D LAVA code has also been successfully used to calculate the VE-U1 spreading area expansion (Allelein et al., 2000).

More refined codes modeling the behaviour of the flow with meshing of the vertical dimension in the flow have also been developed. The 2D CROCO (Michel et al., 2000) and CORFLOW (Wittmaack, 1997) codes have been also satisfactorily validated against the VE-U1 spreading experiment. The CROCO calculation shows a significant influence of the melt surface emissivity, controlling the upper crust thickness, on the stop of the spreading.

A benchmark exercise of spreading codes on VE-U7 is underway.

4.3. Microstructure and thermodynamic modeling

The chemical analyses of the spread melts indicate that there is no sign of heterogeneity within the flow, which has a somehow constant elemental composition. Furthermore, solidification does not occur in the form of a dendritic mushy zone growing from the cold region, but rather as a suspension of solids in the remaining liquid. This configuration is thus similar to that of semisolid alloys (Flemmings, 1991). It has been shown in experiments with transparent simulants (Jeulain et al., 2001) that this is due to the effects of shear on crystallization.

Notwithstanding the chemical element uniform repartition, the microstructure and the phases in presence vary greatly depending on the vertical position, as shown in Fig. 27. These effects (Journeau et al., 1999a, 2001a) have been explained by the variations in cooling rate, and for very thin surface layers ($<100\,\mu m$), the oxidation by air. In the spread lowermost layer (less than 1 mm thick in our cases), which, as it will be developed in Section 4.5, was thermally insulated by a large thermal contact resistance, the solidification was close to thermodynamic equilibrium. A tracer of thermodynamic equilibrium below 1600 °C is the formation of silicates of hafnium, zirconium, and/or uranium, including, at least in VE-U1, a compound close to chernobylite (Pazukhin, 1994), the zirconium–uranium silicate observed in Chernobyl "lavas."

In the bulk of the spread, solidification is quicker (>10 K/s) and diffusion in the solid phase had not enough time to occur. In some cases (e.g. VE-07), the upper interface is characterized by dendritic particles. The threshold between dendritic and equiaxed particles (visible in Fig. 27a and b, respectively) has been related to the ratio between temperature gradient in the melt and particle growth rate (Jeulain, 2001) according to Tiller et al. (1953) theory.

The post-mortem analyses of these tests made with mixtures of a large number of constituents (at least five major chemical elements) have also contributed to the validation of the European corium thermodynamic databases (De Bremaecker et al., 2002).

4.4. Physical properties

As shown by the spreading-code sensitivity-analysis, physical properties can greatly affect the spreading of corium. But, there are a lot of uncertainties in estimating the properties of a mixture of a multicomponent melt and solid particles at high temperatures.

Thermodynamic computations provide, for each temperature (and solidification path) the estimated repartition of phases in corium and the composition of each phase (Journeau et al., 1999a, 2001a). Due to the rapid cooling, there is no macrosegregation between the phases during spreading, as shown in the post-test analyses. The physical properties of a suspension of the calculated phases must thus be estimated.

For the estimation of specific mass, we assume, following Nelson and Carmichael (1979), that the partial molar volume of all the constituent of the liquid phase have no compositional dependence. The molar volume of the liquid or solid phases is thus estimated as the weighed average of the constituent molar volumes. The same procedure is then used for the mixture of the phases in presence.

The evolution of the suspension rheology during solidification can be estimated using the methodology proposed by Ramacciotti et al. (2001). The liquid phase viscosity is estimated in the absence of silica using the approach of Sudreau and Cognet (1997), or using Urbain (1987) model in the presence of silica (silica molecules form networks that affect significantly the melt viscosity). The presence of solid particles is then taken into account by the relationships proposed by Ramacciotti et al. (2001):

$$\eta_{rel} = \exp(2.5C\phi)$$

where η_{rel} is the relative viscosity, i.e. the ratio of the liquid–solid suspension viscosity to the viscosity of the remaining liquid; ϕ the solid volume fraction; C a constant which has been experimentally found

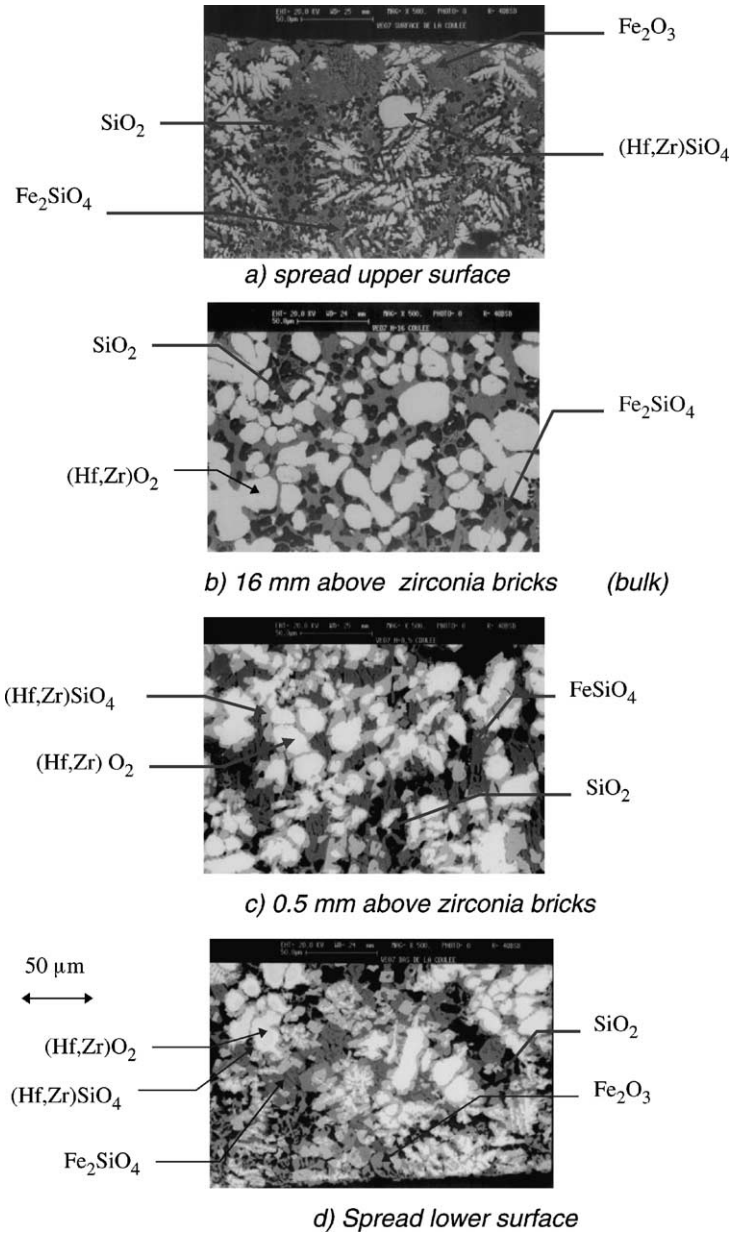

Fig. 27. Evolution of VE-07 microstructure vs. height.

between 3.5 and 8; and Jeulain et al. (2001) proposed to take into account non-Newtonian effects with the following law:

$$C = 1 + \left(\frac{\dot{\gamma}_c}{\dot{\gamma}}\right)^n$$

where $\dot{\gamma}$ is the shear rate; $\dot{\gamma}_c$ is a critical shear rate (found at $325\,s^{-1}$ for Roche (1993) corium viscosity data—Run 34); n is an experimentally fitted exponent ($n = 0.31$ for Roche (1993), Run 34).

It must be noted that heat transfer and fluid flow affect the solidification path and the solid particle shape.

They will thus affect the physical properties of the mixture.

According to the isothermal viscous-gravity model of Huppert (1982), the shear rate at the abscissa z of a flow of height h traveling at the average velocity u is: $\dot{\gamma} = 3(u/h^2)z$. Thus, for the typical front velocities (0.2 m/s) and height (60 mm) encountered in VULCANO tests, the maximum shear rate is of the order of $10\,s^{-1}$. In the reactor case, the characteristic velocities and height are of the order of 6 m/s and 50 cm, respectively (Wittmaack, 1997), so the maximum shear rate is expected to be in the order of $30\,s^{-1}$.

In the THEMA calculation, the constant C is one of the main parameters that are optimized to fit the experimental spreading front evolution. The values of $C = 6.1$ and 6.3 have been found for tests VE-U1 and VE-U7, respectively. Unfortunately, the uncertainties on physical properties and initial conditions in the VULCANO test did not allow to precise the non-Newtonian nature of solidifying corium, contrary to the more analytic works of Roche (1993).

4.5. Spreading over concrete

During test VE-U7, the hydrodynamic initial conditions and corium properties were similar for the flows over refractory ceramic and siliceous concrete. The spreading kinetics were equivalent (see Fig. 28) for the two substrates until the flow over concrete stopped. The overall spreading lengths are of the same magnitude (36 cm versus 45 cm). This result is consistent with the results of S3E 3MDC-Ox1/3MDS-Ox1 tests (Dinh et al., 2000) and COMAS EU 2b (Steinwarz et al., 1999) test. Dinh et al. (2000) attributed the similarity of spreading lengths, although there are violent gas outburst over the concrete channels, to the fact that "the termination of the spreading process is largely governed by solidification at the leading edge rather than on the processes occurring behind the spreading edge." Nevertheless, in the KATS 12 and 13 tests (Engel et al., 2000) the spreading distance was considerably less on concrete (7.5 m) than on ceramic (12 m). It must be noted that in this test the inlet temperature was 100 °C above liquidus contrary to the VULCANO test configurations. Anyhow the difference is below a factor of 2.

Concerning concrete ablation during the two VULCANO tests onto concrete without sustained heating, the following observations were made:

- A preferential penetration of corium in the mortar between the concrete large aggregates.
- Cracking of silica aggregates, probably by thermal stresses, into which corium penetrated.
- Release of carbon oxide from limestone aggregates, forming very light porous stones.
- The sparging gas caused a few "eruptions" on the corium upper surface rather than an homogeneous distribution of gas escape routes.

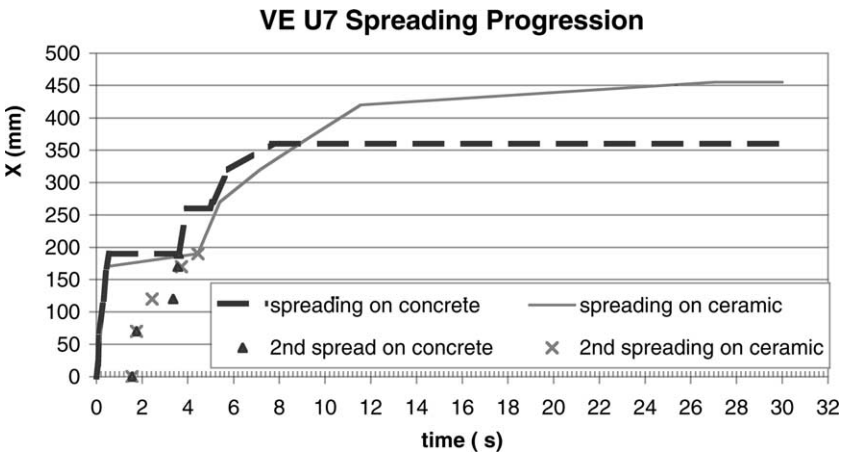

Fig. 28. Evolution of corium front over the two substrates for VE-U7.

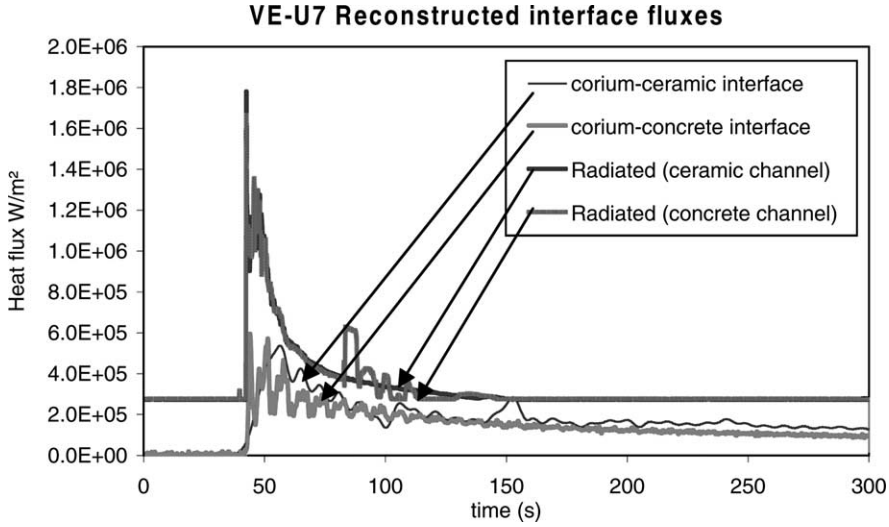

Fig. 29. Comparison of radiated heat flux and reconstructed conduction flux at the substrate upper surface for the two channels of VE-U7.

4.6. Corium–substrate interface

During the spreading tests on refractory or metallic substrates, corium has only very locally attacked the substrate (mainly at the inlet of the spreading plane). Post-test analyses show mainly a penetration of corium in the brick pores with little chemical reaction. The outcome would be different in longer term experiments for which decay heat is simulated. Indeed in this last type of experiment, partial dissolution of the crucible has been observed at VULCANO (Journeau et al., 2001b).

The heat flux at the corium–substrate interface can be estimated using an inverse conduction technique (Raynaud and Bransier, 1986) from temperature measured at various depths inside the substrate. For instance, during the VE-U1 flow, the downward heat flux entering the zirconia bricks was estimated around 200 kW/m^2, whereas the radiated flux at the free surface was around 900 kW/m^2. These values must be compared to the heat flux that is expected in case of perfect contact between two large conducting bodies:

$$\phi = \frac{b_{\mathrm{sub}}}{\sqrt{\pi t}} \left(\frac{b_{\mathrm{cor}} T_{\mathrm{cor}} + b_{\mathrm{sub}} T_{\mathrm{sub}}}{b_{\mathrm{cor}} + b_{\mathrm{sub}}} - T_{\mathrm{sub}} \right)$$

where b is the effusivity (square root of the product conductivity by specific mass by specific heat), t is the time, T is the temperature and cor and sub subscripts refer to corium and substrate, respectively.

In the case of VE-U1, the flux would have been of 500 kW/m^2 after 5 s of contact. This means that a large thermal contact resistance must have been present. It is estimated around 3×10^{-3} to 6×10^{-3} K m^2/W and is attributed to the shrinkage at solidification of the lower crust as observed in metallic casting (Loulou et al., 1999).

For VE-U7, we observed that the heat fluxes transmitted to both substrates (Fig. 29) are of the same order of magnitude (300–400 kW/m^2) and much lower than the values for perfect contact, so the thermal contact resistance seems to be more controlled by the corium than the substrate. It has also be noted that the radiated heat flux is significantly higher than the heat flux transmitted to the substrate. THEMA calculations indicates that with a thermal contact resistance of the order of 1×10^{-3} and 5×10^{-3} K m^2/W, respectively for concrete and ceramic substrate yield to satisfactory fits of the substrate temperature evolution.

4.7. Gases

One of the main differences observed in these tests between simulant and prototypic materials is the

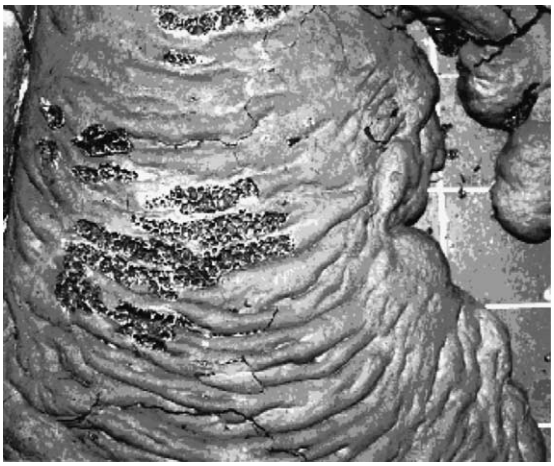

Fig. 30. View of the VE-U5 corium spreads showing holes at the surface.

presence of large porosities in the VE-U1, VE-U5 and VE-U7 spreads. It must be noted that for simulant test VE-07, very close in composition and operating conditions to test VE-U1 (actually it was the rehearsal of VE-U1 with hafnia instead of zirconia), only a small porosity was observed.

The tests over concrete showed that porosity is slightly affected by the presence or absence of an external gas source. This could mean that void fraction is almost independent of gas flow rate.

The porosities over refractory bricks cannot be only attributed to air flowing out of the substrate pores under the effect of thermal expansion, since it also occurred when the substrate was made of steel (VE-U5) or dense zirconia (VE-U7). Fig. 30 shows a view of VE-U5 spread over a steel plate. Part of the crust have been destroyed by a gas pressure below it. Under the portion of crust that remained intact, a powder mainly made of U_3O_8 and SiO_2 have been observed. The inner side of the crust had a structure reminding convection cells.

Several evidences are consistent with an hypothesis of oxygen exchange processes during the experiment leading to the local formation of volatile UO_3 and SiO. Further analyses are underway to investigate this hypothesis and assess its consequence on corium physical properties and behavior.

An associated difference between prototypic and simulant melts is that many of the simulant melt displayed uncracked surfaces whereas in our prototypic material tests, the corium surface was always cracked. This features would be favorable for corium cooling by top-flooding.

4.8. Consequences for reactor case

The spreading tests conducted in the VULCANO facility, but also in the CARLA and FARO facilities lead to a validation of spreading models and codes with prototypic material with a large variability of corium composition and of initial and boundary conditions.

Konovalikhin et al. (2000) applied the scaling simplified model to some EPR reference cases (300–350 t of corium poured in 30–90 s) and showed that the corium final thickness should be of the order of 30 cm, i.e. spreading covering the hole chamber surface (within a factor of 2 uncertainty).

Application to reactor case of the THEMA code (Steinwarz et al., 2002) showed that “even for very conservative conditions, [dry] spreading is not a problem” for the EPR core catcher concept in which corium is mixed with sacrificial concrete in the reactor pit before spreading. This is in total agreement with the experimental observations that a high-temperature mixture presenting a large solidification range has a good spreadability.

Uncertainties on the ability of corium to spread in the reactor cases remains only in the following cases: spreading of large masses of an UO_2–ZrO_2 mixture with a small solidification range and hence, for which less enthalpy has to be removed before immovability and the spreading under water where rapid quenching can lead to a debris bed through which the melt flows (Tribble, 1991). In both configuration the crust strength is an important parameter for which there is little data and very large scale experiments are needed to enable crust breaches.

One other important outcome of these tests is that for ceramic core catchers, as, e.g. the core catcher installed at Tian Wan (Asmolov et al., 2002), even in the absence of extraneous gas sources (as above concrete), there is a production of gas inside the corium or due to exchanges between corium melt and atmosphere. This gas flow creates a significant porosity and will modify natural convection inside melt pools.

5. Conclusions

Twelve spreading tests have been performed at the VULCANO facility, including five with prototypic corium containing up to 80 wt.% of UO_2 which are representative of either in-vessel corium or of the products of a corium–concrete interaction in the reactor pit. They have shown with real materials the promises of spreading concepts for corium management in the hypothetical case of a nuclear reactor severe accident. Spreading to thin corium thickness has been obtained with corium–concrete mixtures. It has been experimentally verified that corium spreading and concrete ablation are temporally disconnected and that the emulsion of a small fraction of metal in oxidic corium does not sediment during the small time of spreading, therefore disconnecting the phenomena.

Spreading codes and models have been validated to the extent permitted by the large uncertainties on corium physical properties in the solidification range. Having better physical property data is one of the major current R&D need in order to validate precisely corium codes and models.

Important differences have been observed between prototypic and simulant materials especially for the physico-chemistry with respect to oxygen exchange processes.

For the complete validation of the spreading concepts, further experiments are needed to study the effects of spreading under water and to analyze the long-term effects, for which the slowly diminishing internal heat generation must be simulated. Nevertheless, applications of the validated spreading codes and models to reactor scale clearly show the spreading concept potentialities.

Acknowledgements

The work and efforts of the whole VULCANO team are greatly acknowledged. Some of the described experiments were part of the Corium Spreading and Coolability project of the European Commission's 4th Framework Program (Contract FI4S-CT96-0041) and of the ECOSTAR (Ex-vessel Core melt Stabilization Research) project of the European Commission's 5th Framework Program (Contract FIKS-CT1999-0003). The sponsorship of the Institut de Protection et de Sûreté Nucléaire (IPSN) for some of the described tests is gratefully acknowledged.

References

Allelein, H.-J., Breest, A., Spengler, C., 2000. Simulation of core melt spreading with LAVA: theoretical background and status of validation. Wissenschaftliche Berichte FZKA 6475, 189–200.

Asmolov, V.G., Zagryazkhin, V.N., Isaev, V.N., Semenov, I.M., Vishnevskii, V.Yu., D'yakov, E.K., Khabenskii, V.B., Bechta, S.V., Granovskii, V.S., Udalov, Yu.P., 2002. Choice of buffer material for the containment trap for VVER-1000 core melt. Atomic Energy 92, 5–14.

Broughton, J.M., Kuan, P., Petti, D.A., Tolman, E.L., 1989. A scenario of the Three Mile Island unit 2 accident. Nucl. Technol. 87, 34–53.

Cas, R.A.F., Wright, J.V., 1988. Volcanic Successions, Modern and Ancient. Chapman & Hall, London, p. 67.

Chevalier, P.Y., Fischer, E., Cheynet, B., Rivet, A., Cénérino, J., 1997. Global thermodynamic approach of the molten core–concrete interaction (MCCl) and selected applications in the nuclear field. J. Chim. Phys. PCB 94, 849–860.

Cognet, G., Journeau, C., Jégou, C., 1995. Infrared thermography for measuring the surface temperature of an oxidic melt. In: Proceedings of the International Symposium on Radiative Heat Transfer, Kusadasi, Turkey, August 14–18, 1995.

Cognet, G., Laffont, G., Jégou, C., Pierre, J., Journeau, C., Sudreau, F., Roubaud, A., 1999. Utilisation d'un four tournant à arc plasma transféré pour fondre et couler des mélanges d'oxydes autour de 2000 °C. Ann. Pharm. Fr. 57, 131–136.

Cognet, G., Seiler, J.-M., Szabo, I., Latché, J.-C., Spindler, B., Humbert, J.-M., 1997. La récupération du corium hors cuve. Rev. Gén. Nucl. 1, 38–43.

Cohen, I., Schaner, B.E., 1963. A metallographic and X-ray study of the UO_2–ZrO_2 system. J. Nucl. Mater. 9, 18–52.

De Bremaecker, A., Barrachin, M., Jacq, F., Defoort, F., Mignanelli, M., Chevalier, P.Y., Cheynet, B., Hellmann, S., Funke, F., Journeau, C., Piluso, P., Marguet, S., Hozer, Z., Vrtilkova, V., Belovsky, L., Sannen, L., Verwert, M., Duvigneaud, P.H., Mwanba, K., Bouchama, H., Ronneau, C., 2002. European nuclear thermodynamic database validated and applicable in severe accident codes (ENTHALPY). In: Van Goetem, G., Zurita, A., Martin, B.J., Manolatos, P., Bischoff, H. (Eds.), FISA 2001 EU Research in reactor safety, Office Official Publications European Communities, Luxembourg, pp. 261–273.

Dinh, T.N., Dong, W.G., Green, G.A., Nourgaliev, R.R., Sehgal, B.R., 1997. Melt jet attack of the reactor vessel wall: phenomena and prediction method. In: Proceedings of the Eighth International Topical Meeting Nuclear Reactor Thermal Hydraulics, Kyoto, Japan, vol. 2, pp. 612–619.

Dinh, T.N., Konovalikhin, M., Sehgal, B.R., 2000. Core melt spreading on a reactor containment floor. Prog. Nucl. Energy 36, 405–468.

Duchatelle, L., Vautrey, J., 1964. Détermination des coefficients de convection d'un alliage NaK en écoulement turbulent antre plaque parallèles. Int. J. Heat Mass Transfer 7, 1017–1031.

Eberlé, P., 1997. Modélisation Physique et Numérique de l'étalement d'un fluide avec solidification dans le cadre des etudes de sûreté pour les réacteurs à eau sous pression, Ph.D. Thesis, Université Joseph Fourier, Grenoble, France.

Engel, G., Fieg, G., Massier, H., Stegmaier, U., Schütz, W., 2000. KATS experiments to simulate corium spreading in the EPR core catcher concept. Wissenschaftliche Berichte FZKA 6475, 148–155.

Fieg, G., Huber, F., Werle, H., Wittmaack, R., 1996. Simulation experiments on the spreading behaviour of molten core melts. In: Proceedings of the National Heat Transfer Conference, Houston, TX.

Fink, J.H., Griffiths, R.W., 1990. Radial spreading of viscous-gravity currents with solidifying crust. J. Fluid Mech. 221, 485–509.

Flemmings, M.C., 1991. Behavior of metal alloys in the semisolid state. Metall. Trans. 22A, 957–981.

Greene, G.A., Finrock, C., Klages, J., Schwarz, C.E., 1988. Experimental studies on melt spreading, bubbling heat transfer and coolant layer boiling. In: Proceedings of the 16th Water Reactor Safety Meeting, NUREG/CP-0096, pp. 341–358.

Huppert, H.E., 1982. The propagation of 2 dimensional and axisymmetric viscous-gravity currents over a rigid horizontal surface. J. Fluid Mech. 121, 43–58.

Jégou, C., Boccaccio, E., Journeau, C., Piluso, P., Monerris, J., 2001. Induction heating simulation of residual power in the VULCANO facility. In: Dughiero, F., Lupi, S. (Eds.), Proceedings of the International Symposium Heating by Internal Sources, SGE Ditoriali, Padova, Italy, pp. 253–260.

Jégou, C., Cognet, G., Roubaud, A., Gatt, J.-M., Laffont, G., Kassabji, F., 1998. Plasma transferred arc rotary furnace for corium melting. J. High Temp. Mater. Proc. 1, 409–420.

Jeulain, G., 2001. Rhéologie des mélanges en cours de solidification sous cisaillement, application au corium, DRT dissertation, Ecole Nationale Supérieure de Céramique Industrielle, Limoges, France.

Jeulain, G., Journeau, C., Benyahia, L., Tassin, J.F., Abélard, P., 2001. Rhéologie de mélanges en cours de solidification, Actes 36° colloque du Groupe Français de Rhéologie, Marne-la-Vallée, France.

Journeau, C., Jung, Y., Pierre, J., 1998. Visualization of a 2000 °C melt spreading over a plane. In: Proceedings of the Eighth International Symposium Flow Visualization, Sorrento, Italy.

Journeau, C., Gatt, J.-M., de Palma, G., 1999b. Transient effects in corium temperature measurements. In: Proceedings of the Ninth International Topical Meeting Nuclear Reactor Thermalhydraulics, NURETH 9, San Francisco.

Journeau, C., Piluso, P., Cranga, M., 2001b. Transferts thermiques lors de la solidification lente d'un bain d'oxydes fondus. In: Castelain, C., Delaunay, D. (Eds.), Actes Congrès SFT. Elsevier, Paris, pp. 371–376.

Journeau, C., Sudreau, F., Gatt, J.-M., Cognet, G., 1999a. Thermal, physico-chemical and rheological boundary layers in multi-component oxidic melt spreads. Int. J. Therm. Sci. 38, 879–891.

Journeau, C., Sudreau, F., Magne, S., Cognet, G., 2001a. Physico-chemical analyses and solidification path reconstruction of multi-component oxidic spread melts. Mater. Sci. Eng. A 299, 249–266.

Konovalikhin, M.J., Dinh, T.N., Nourgaliev, R.R., Sehgal, B.R., Fischer, M., 2000. The scaling model of core melt spreading: validation refinement and reactor application. Wissenschaftliche Berichte FZKA 6475, 246–258.

Loulou, T., Artyukhin, E.A., Bardon, J.P., 1999. Estimation of thermal contact resistance during the first stages of metal solidification. Int. J. Heat Mass Transfer 42, 2119–2142.

Michel, B., Piar, B., Babik, F., Latché, J.-C., Guillard, G., De Pascale, C., 2000. Synthesis of the validation of CROCO v1 spreading code. Wissenschaftliche Berichte FZKA 6475, 235–246.

Nelson, S.A., Carmichael, I.S.E., 1979. Partial molar volumes of oxide components in silicate melts. Contrib. Mineral Petrol. 71, 117–124.

Nie, M., 2000. Application of sacrificial concrete for the retention and conditioning of molten corium in the EPR core melt retention concept. Wissenschaftliche Berichte FZKA 6475, 527–534.

Pazukhin, E.M., 1994. Fuel-containing lavas of chernobyl NPP 4th block: topography, physicochemical properties and formation scenarios. Radiochemistry 36, 109–154.

Piluso, P., Journeau, C., Cognet, G., Magallon, D., Seiler, J.-M., 2001. Importance of prototypic-corium experiments for severe accident research. In: Proceedings of the ICONE9 International Conference, Nuclear Engineering, Nice, France.

Ramacciotti, M., Sudreau, F., Journeau, C., Cognet, G., 2001. Viscosity models for corium melts. Nucl. Eng. Des. 204, 377–389.

Raynaud, M., Bransier, J., 1986. A new finite-difference method for the nonlinear inverse heat conduction problem. Num. Heat Transfer 9, 27–42.

Roche, P., 1993. Viscosity of corium concrete mixtures at high temperatures. Argonne Nat. Lab. Rep. ACE-TR-C37.

Ruh, R., Garett, H.J., Domagala, R.F., Tallan, N.M., 1968. The system zirconia–hafnia. J. Am. Ceram. Soc. 51, 23–27.

Sappok, M., Steinwarz, W., 1999. Large scale experiments on ex-vessel core melt behavior. Nucl. Technol. 125, 363–370.

Spindler, B., Veteau, J.M., Brayer, C., Cranga, M., De Cecco, L., Montanelli, P., Pineau, D., 2000. Assessment of THEMA code against spreading experiments. Wissenschaftliche Berichte FZKA 6475, 221–245.

Steinwarz, W., Häfner, W., Alkan, Z., Fischer, M., 1999. Groβexperimente mit repräsentativer Kernschmelze im Hinblick auf die Beherrschung eines Kernschmelzunfalls. Jahrestagung Kerntech 44, 441–736.

Steinwarz, W., Koller, W., Häffner, W., Journeau, C., Seiler, J.-M., Froment, K., Cognet, G., Goldstein, S., Fischer, M., Hellmann, S., Eddi, M., Alsmeyer, H., Allellein, H.-J., Spengler, C., Bürger, M., Sehgal, B.R., Koch, M.K., Alkan, Z., Petrov, J.B., Gaune-Escard, M., Weiss, F.-P., Bandini, G., 2002. Ex-vessel core melt stabilization research (ECOSTAR). In: Van Goetem, G., Zurita, A., Martin Bermejo, J., Manolatos, P., Bischoff, H. (Eds.), FISA 2001 EU Research in reactor safety, Office Official Publications European Communities, Luxembourg, pp. 274–285.

Sudreau, F., Cognet, G., 1997. Corium viscosity modelling above liquidus temperature. Nucl. Eng. Des. 178, 269–277.

Suzuki, H., Matsumoto, T., Sakaki, I., Mitadera, T., Matsumoto, M., Zama, T., 1993. Fundamental experiment and analysis for melt spreading on concrete floor. Proc. ASME/JSME Nucl. Eng. Conf. 1, 403–407.

Tiller, W.A., Jackson, K.A., Rutter, J.W., Chalmers, B., 1953. The redistribution of solute atoms during the solidification of metals. Acta. Metall. 1, 428–437.

Tribble, G.W., 1991. Underwater observations of active lava flows from Kilauea volcano. Hawaii Geol. 19, 633–636.

Tromm, W., Foit, J.J., Magallon, D., 2000. Dry and wet spreading experiments with prototypic material at the FARO facility and theopretical analysis. Wissenschaftliche Berichte FZKA 6475, 178–188.

Urbain, G., 1987. Viscosity estimation of slags. Steel Res. 58, 111–116.

Vetau, J.M., Wittmaak, R., 1996. CORINE experiments and theoretical modelling. In: Van Goetem, G., Balz, W., Della Loggia, E. (Eds.), FISA 95 EU research on severe accidents, Office Official Publications European Communities, Luxembourg, pp. 271–285.

Weisshäupl, H.A., 1999. Severe accident mitigation concept of EPR. Nucl. Eng. Des. 187, 35–45.

Wittmaack, R., 1997. Numerical simulation of free surface flows. Nucl. Technol. 119, 158–180.